

FIRING PATTERNS AND BIFURCATION ANALYSIS OF NEURONS UNDER ELECTROMAGNETIC INDUCTION

QIXIANG WEN AND SHENQUAN LIU*

School of Mathematics
South China University of Technology
Guangzhou 510640, China

BO LU

School of Science and Mathematics
Henan Institute of Science and Technology
Xinxiang 453003, China

ABSTRACT. Based on the three-dimensional endocrine neuron model, a four-dimensional endocrine neuron model was constructed by introducing the magnetic flux variable and induced current according to the law of electromagnetic induction. Firstly, the codimension-one bifurcation and Interspike Intervals (ISIs) analysis were applied to study the bifurcation structure with respect to external stimuli and parameter k_0 , and two dynamical behaviors were found: period-adding and period-doubling bifurcation leading to chaos. Besides, Hopf bifurcation was specially discussed corresponding to the transformation of the state. Secondly, the different firing patterns such as regular bursting, sub-threshold oscillations, fast spiking, mixed-mode oscillations (MMOs) etc. can be observed by changing the external stimuli and the induced current. The neuron model presented more firing activities under strong coupling strength. Finally, the codimension-two bifurcation analysis shown more details of bifurcation. At the same time, the Bogdanov-Takens bifurcation point was also analyzed and three bifurcation curves were derived.

1. Introduction. The electrical activities of neurons are the basis of transmitting information in the nervous system. Especially, the excitability of neurons is sensitive to many factors, such as the neuronal intracellular and extracellular ion concentration, environmental noise, temperature and so on. The single neuron can exhibit multiple firing patterns under the external stimulus, while the transformation between different firing patterns corresponds to the bifurcation of models, such as the pancreas β cells increase the duty cycle as blood sugar levels rise [17]. Duan et al. study the bifurcation associated with the transition of bursting patterns in the Chay model [5]. MMOs corresponding to more complex bifurcations have also been extensively investigated through geometric singular perturbation theory [25]. Teka Krasimira et al. discuss in detail the transition from plateau to pseudo-plateau bursting by using two-parameter bifurcation [22]. It can be seen that the bifurcation theory is a powerful tool to analyze the firing patterns of neurons.

2020 *Mathematics Subject Classification.* Primary: 37N25, 34C23; Secondary: 37N30, 92C20.
Key words and phrases. Electromagnetic induction, bursting, fast-slow dynamics, bifurcation.
The first author is supported by NSF of China under Grant Nos. 11872183 and 11572127.

* Corresponding author: Shenquan Liu.

According to Faraday's law of electromagnetic induction, the action potential of excitable neurons can generate the magnetic field in the medium, and the magnetic field can influence the neurons in turn. Interestingly, Barry et al. have found the magnetic field, indicating that the magnetic field exists generated by action potential [1]. The exogenous magnetic field has obvious influence on the electrical activity of neurons [20][21]. Therefore, it is a direction to study theoretically the dynamic behavior of neurons under electromagnetic induction. Recently, many researchers have begun to put attention to the dynamics of electromagnetic induction on neurons and neural networks [4]. Li et al. build a mathematical model under electromagnetic radiation to study the variation of firing rhythms of neurons [11]. Then, Lv and Ma introduce a magnetic flux variable and the feed-back current on the membrane potential on the Hindmarsh-Rose (HR) neuron model and study the electrical activities [14]. On this basis, Mvogo et al. investigate the spatiotemporal formation of patterns in a diffusive FitzHugh-Nagumo network under the effects of electromagnetic induction [16]. Further, most investigations focus on the simplified neuronal models [15][9], while the effects of electromagnetic induction on the biological neuron models are relatively little considered.

Bursting is characteristic of the nervous system. Bursting oscillations play an important role in information transmission of the nervous system. For this reason, many models have been established to study different bursting activities [12]. Studies show that bursting consists of a fast process and a slow process: the generation of action potentials and modulates fast variables [18]. Thus, the fast process is separated from the slow process, then we can analyze the firing behavior of the fast subsystem, which is called fast-slow dynamics analysis [18]. Izhikevich uses this method to topologically classify bursting types [8]. Moreover, Bertram has discussed the application of fast-slow dynamics analysis in different oscillations in detail, such as relaxation oscillations, neuronal bursting oscillations, canard oscillations, and MMOs [2].

In this paper, taking the endocrine model [23] as the research object, we aim to explore the bifurcation and firing rhythms of neurons under electromagnetic induction and external forcing direct current. The organization of this paper is as follows. In Section 2, we describe the endocrine model and introduce electromagnetic induction. In Section 3, for one-parameter bifurcation, we study the codimension-one and Interspike Intervals bifurcation, and the first Lyapunov coefficient is computed to judge the Hopf bifurcation stability. At the same time, the chaotic region of the system is discussed through the first and second Lyapunov exponents. In Section 4, according to the difference of coupling strength between membrane potential of the neuron and magnetic flux, the firing behaviors of the neuron model are discussed. In Section 5, we also explore two-parameter bifurcation analysis in the (I_{ext}, k_0) phase plane, and investigate the Bogdanov-Takens bifurcation. Furthermore, we get three bifurcation curves: a saddle-node bifurcation curve, a Hopf bifurcation curve and a homoclinic bifurcation curve.

2. Model description. To study the plateau-bursting patterns, Tsaneva-Atanasova et al. have constructed a generic simplified endocrine model based on elements drawn from several published models [23]. Here we introduce magnetic flux across the membrane and feedback current as induction current resulted from the variation of magnetic flux and field, then we get the following system:

TABLE 1. Parameter values used in this paper

Parameter	Value	Parameter	Value	Parameter	Value
f_c	0.0001	g_{Ca}	0.81nS	k_{PMCA}	$20s^{-1}$
d_{cell}	$10\mu m$	$g_{K(Ca)}$	0.2nS	τ_n	$0.03s^{-1}$
V_{ml}	-22.5mV	g_K	2.25nS	α	1
V_K	-65mV	k_0	0.01	k_1	1
V_{Ca}	0mV	β	0.0001	k_2	3

$$\begin{cases} \frac{dV}{dt} = -(I_{Ca} + I_K + I_{K_{Ca}} + k_0 V \rho(\varphi) + I_{ext}) / C_m, \\ \frac{dn}{dt} = (n_\infty(V) - n) / \tau_n, \\ \frac{dc}{dt} = -f_c (\theta g_{Ca} m_\infty^2(V) (V - V_{Ca}) + k_{PMCA} c), \\ \frac{d\varphi}{dt} = k_1 V - k_2 \varphi, \end{cases} \quad (1)$$

where variable V is the membrane potential, n is the gating variables for the voltage-gated potassium, c represents the free Ca^{2+} concentration in the cytosol the corresponding fluxes and φ is magnetic flux across the membrane. The ionic currents I_{Ca} , I_K and $I_{K_{Ca}}$ represent inward calcium current, delayed-rectifier potassium current and calcium-activated potassium ion current, respectively. I_{ext} is the external forcing direct current. $C_m = 10^{-5} \times A_{cell}$ is the membrane capacitance; τ_n is the activation time constant for the delayed rectifier channel; n_∞ is the steady-state function for gating variable n ; f_c is the fraction of free to total cytosolic Ca^{2+} ; $\theta = 10^5 (2 \times 9.65 \times A_{cell})^{-1}$ is a factor that converts current to flux, where $A_{cell} = \pi \times d_{cell}^2$ is the surface area of cell; k_{PMCA} is the plasma membrane Ca^{2+} ATPase pump rate. The expressions of ion current are as following:

$$\begin{aligned} I_{Ca} &= g_{Ca} m_\infty^2 (V - V_{Ca}), \\ I_K &= g_K n (V - V_K), \\ I_{K_{Ca}} &= g_{K(Ca)} s_\infty (V - V_K), \end{aligned}$$

The steady-state activation functions are described as the following equations:

$$\begin{aligned} m_\infty(V) &= (1 + \exp((V_{ml} - V)/12))^{-1}, \\ n_\infty(V) &= (1 + \exp((-V/8)))^{-1}, \\ s_\infty(c) &= c^4 / (c^4 + 1.25^4). \end{aligned}$$

In addition, other fixed parameters used in this paper are given in Table 1.

In this paper, the term of the $k_0 V \rho(\varphi)$ describes the feedback current as induction current results from the variation of magnetic flux and k_0 is feedback gain. $\rho(\varphi) = \alpha + 3\beta\varphi^2$ is a magnetic flux-controlled memristor, which is equivalent to memory conductance and is used to describe the coupling relation between membrane potential of the neuron and magnetic flux, α and β are fixed parameter values [14]. Parameter k_1 and k_2 are the interaction between membrane potential and magnetic flux [14].

3. One-parameter bifurcation analysis. Usually, using external stimuli is a common method to explore the firing patterns of neurons. Meanwhile, we also aim

to study the influence of electromagnetic induction on the firing rhythm of neuron model, so we choose I_{ext} and k_0 as bifurcation parameters. Then Codimension-one and ISIs bifurcation are used to explore the bifurcation structure of the system (1).

3.1. Codimension-one bifurcation analysis. The dynamical properties of external forcing current are first investigated. Equilibrium is an important part in understanding the behavior of a dynamical system. To find the equilibrium, we can rewrite the system (1) as following:

$$\begin{cases} V' = F_1(V, n, c, \varphi), \\ n' = F_2(V, n, c, \varphi), \\ c' = F_3(V, n, c, \varphi), \\ \varphi' = F_4(V, n, c, \varphi), \end{cases} \quad (2)$$

where

$$\begin{aligned} F_1 &= -(g_{Ca}m_\infty^2(V - V_{Ca}) + g_K n(V - V_K) \\ &\quad + g_{K(Ca)}s_\infty(V - V_K) + k_0 V \rho(\varphi) + I_{ext})/C_m, \\ F_2 &= (n_\infty - n)/\tau_n, \\ F_3 &= -f_c(\theta g_{Ca}m_\infty^2(V - V_{Ca}) + k_{PMCA}c), \\ F_4 &= k_1 V - k_2 \varphi, \end{aligned}$$

where $m_\infty, s_\infty, n_\infty, \rho(\varphi)$ are the same as defined in Section 2.

Let $F_1 = F_2 = F_3 = F_4 = 0$, then we get the expressions of n, c, φ with respect to V : $n(V) = n_\infty(V)$, $c(V) = \theta g_{Ca}m_\infty(V)^2(V_{Ca} - V)/k_{PMCA}$, $\varphi(V) = k_1 V/k_2$. Next, we put these into $F_1 = 0$, so we can easily obtain the expression of equilibrium with respect to I_{ext} :

$$\begin{aligned} I_{ext} &= -g_{Ca}m_\infty^2(V)(V - V_{Ca}) - g_K n_\infty(V)(V - V_K) \\ &\quad - g_{K(Ca)}s_\infty(c(V))(V - V_K) - k_0 V \rho(\varphi(V)). \end{aligned} \quad (3)$$

We can calculate the codimension-one bifurcation points by using MATCONT, see Figure.1(a). It can be seen there are three bifurcation points on the curve, namely H, LP₁ and LP₂. H represents Hopf bifurcation, where $I_{ext} = -0.196411$, LP₁ and LP₂ are fold bifurcation points at $I_{ext} = 0.831046$, $I_{ext} = 0.703546$, respectively. The blue curve indicates stable fixed points, and the black curve is unstable fixed points. For $I_{ext} < -0.196411$, the system (2) has only one stable equilibrium and there exist quiescent state; Then the system (2) changes its stability from stable to unstable through Hopf bifurcation at $I_{ext} = -0.196411$, it means the system (2) enter firing state; For $0.703546 < I_{ext} < 0.831046$, the system (2) has three equilibriums through fold bifurcation LP₂, then another fold bifurcation occurs at LP₁ as we increase the value of parameter I_{ext} ; Finally, for $I_{ext} > 0.831046$, there is only one stable equilibrium.

Now, we only consider the effect of intensity of induced current and set I_{ext} to zero to obtain the S-type bifurcation curve with respect to parameter k_0 in the same way, as shown in Figure.1(b). there are two fold bifurcation points on the curve occurring on $k_0 = -0.007763$ and $k_0 = 2.54 \times 10^{-22}$ (not drawn). Hopf bifurcation point appears at $k_0 = 0.012850$. The bifurcation structure is similar to the previous ones, so it will not be explained in detail.

The transformation between the quiescent state and the firing state is related to these bifurcation points. Therefore, we need to verify the dynamical properties of

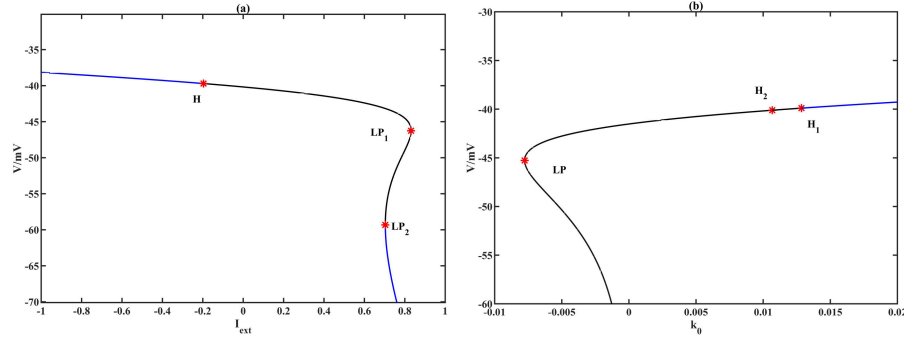


FIGURE 1. (a) The one-parameter bifurcation versus I_{ext} in improved endocrine model. H is Hopf bifurcation point, LP_i ($i = 1, 2$) are fold bifurcation points. (b) The bifurcation diagram of k_0 . LP is fold bifurcation point, H_1 is Hopf bifurcation point, H_2 is neutral saddle.

bifurcation points. The first Lyapunov coefficient determines whether Hopf bifurcation is supercritical or subcritical. It is clear that Hopf bifurcation is supercritical (or subcritical), if the first Lyapunov coefficient is negative (or positive). We take parameter I_{ext} as an example to verify the dynamical properties of these bifurcation points.

Typically, we need to calculate the Jacobian matrix of the system (2), and the Jacobian matrix can be express as:

$$A = \begin{pmatrix} \frac{\partial F_1}{\partial V} & \frac{\partial F_1}{\partial n} & \frac{\partial F_1}{\partial c} & \frac{\partial F_1}{\partial \varphi} \\ \frac{\partial F_2}{\partial V} & \frac{\partial F_2}{\partial n} & \frac{\partial F_2}{\partial c} & \frac{\partial F_2}{\partial \varphi} \\ \frac{\partial F_3}{\partial V} & \frac{\partial F_3}{\partial n} & \frac{\partial F_3}{\partial c} & \frac{\partial F_3}{\partial \varphi} \\ \frac{\partial F_4}{\partial V} & \frac{\partial F_4}{\partial n} & \frac{\partial F_4}{\partial c} & \frac{\partial F_4}{\partial \varphi} \end{pmatrix}, \quad (4)$$

For the bifurcation points, we use the matrix (4) and the system (2) to calculate the equilibrium, then we can get the coordinate of bifurcation points. When $I_{ext} = -0.196411$, the coordinate of equilibrium of the system (2) is $(V, n, v, \varphi) = (-39.709558, 0.006939, 0.98244, -13.236519)$, hence we can obtain the corresponding eigenvalues of the Jacobian matrix A are $\lambda_1 = -17.850777$, $\lambda_2 = -2.785812$, and $\lambda_{3,4} = \pm 0.752697i$. Therefore, Hopf bifurcation occurs at point H. For $I_{ext} = 0.831046$, the coordinate of equilibrium of the system (2) is $(-46.262568, 0.00307, 0.454643, -15.420856)$. And the corresponding eigenvalues of the Jacobian matrix A are $\lambda_1 = -29.52063$, $\lambda_2 = -2.96421$, $\lambda_3 = 11.504217$ and $\lambda_4 = 0$. Consequently, there is a fold bifurcation. So LP_1 is tested. At point LP_2 (when $I_{ext} = 0.703546$), the equilibrium of the system (2) is $(-59.325527, 0.000601, 0.078164, -19.775176)$. the corresponding eigenvalues of the Jacobian matrix A are $\lambda_1 = -33.030555$, $\lambda_2 = -2.7488253$, $\lambda_3 = 0.00146518$ and $\lambda_4 = 0$. Accordingly, a fold bifurcation occurs at LP_2 .

Besides, it is necessary to calculate the first Lyapunov coefficient [10], since it determines the stability of Hopf bifurcation. First, we can calculate the Jacobian

matrix at point H:

$$A|_H = \begin{pmatrix} 15.698748885 & -18112.944392 & -1310.458331 & -0.33461776 \\ 0.02871016577 & -33.3333333 & 0 & 0 \\ 0.0002149731 & 0 & -0.002 & 0 \\ 1 & 0 & 0 & -3 \end{pmatrix},$$

which has a pair of conjugate eigenvalues $\lambda_{3,4} = \pm i\omega$, where $\omega = 0.752697$. Let

$$q = \begin{pmatrix} 0.951504640658750 \\ 8.191181 \times 10^{-4} - 1.8496434 \times 10^{-5}i \\ 7.22063 \times 10^{-7} - 2.71751 \times 10^{-4}i \\ 0.298384796 - 0.0748644585i \end{pmatrix},$$

$$p = \begin{pmatrix} -1.0504305 - 0.036749397i \\ 570.951488 + 7.07658770255i \\ 68.84013411 - 1828.634384i \\ 0.1111930307 - 0.023799224i \end{pmatrix},$$

which satisfy $Aq = i\omega q$, $A^T p = -i\omega p$ and $\langle p, q \rangle = 1$. Then, we need to move the equilibrium of the system (2) to the origin of the coordinate for computing the first Lyapunov coefficient. Then, we will make the transformation:

$$\begin{cases} V = \xi_1 + V_0, \\ n = \xi_2 + n_0, \\ c = \xi_3 + c_0, \\ \varphi = \xi_4 + \varphi_0, \end{cases}$$

where V_0 , n_0 , c_0 and φ_0 are coordinate of H point. By this transformation, the system (2) is converted into this follow:

$$\begin{cases} \dot{\xi}_1 = (-g_{Ca}m_\infty^2(\xi_1 + V_0)(\xi_1 + V_0 - V_{Ca}) - g_K(\xi_2 + n_0)(\xi_1 + V_0 - V_K) \\ \quad - g_{K(Ca)}s_\infty(\xi_3 + c_0)(\xi_1 + V_0 - V_K) - k_0(\xi_1 + V_0)\rho(\xi_4 + \varphi_0) - I_{ext})/C_m, \\ \dot{\xi}_2 = (n_\infty(\xi_1 + V_0) - (\xi_2 + n_0))/\tau_n, \\ \dot{\xi}_3 = -f_c(\theta g_{Ca}m_\infty^2(\xi_1 + V_0)(\xi_1 + V_0 - V_{Ca}) + k_{PMCA}(\xi_3 + c_0)), \\ \dot{\xi}_4 = k_1(\xi_1 + V_0) - k_2(\xi_4 + \varphi_0), \end{cases} \quad (5)$$

Now, consider the system:

$$\dot{x} = Ax + F(x), \quad x \in \mathbf{R}^4$$

where $A = A|_H$, $F(x) = \frac{1}{2}\mathbf{B}(x, x) + \frac{1}{6}\mathbf{C}(x, x, x) + \mathbf{O}(\|x^4\|)$, at the neighborhood of x , $\mathbf{B}(x, x)$ and $\mathbf{C}(x, x, x)$ are symmetric multilinear vector functions which take on the planar vectors $x = (x_1, x_2, x_3, x_4)^T$, $y = (y_1, y_2, y_3, y_4)^T$ and $z = (z_1, z_2, z_3, z_4)^T$. In coordinates, we have

$$\mathbf{B}_i(x, y) = \sum_{j,k=1}^4 \frac{\partial^2 F_i(\xi, 0)}{\partial \xi_j \partial \xi_k} \Big|_{\xi=0} x_j y_k \quad i = 1, 2, 3, 4,$$

$$\mathbf{C}_i(x, y) = \sum_{j,k,l=1}^4 \frac{\partial^3 F_i(\xi, 0)}{\partial \xi_j \partial \xi_k \partial \xi_l} \Big|_{\varepsilon_-} x_j y_k z_l \quad i = 1, 2, 3, 4,$$

where $\xi = (\xi_1, \xi_2, \xi_3, \xi_4)$.

It is not complicated to compute

$$B(x, y) = \begin{pmatrix} 3.4802419x_1y_1 - 716.19724391(x_1y_2 + x_2y_1) - 51.8163509(x_1y_3 + x_3y_1) \\ + 0.00842663(x_1y_4 + x_4y_1) - 1054.40592x_3y_3 + 0.0252798899x_4y_4 \\ 0.00353896895x_1y_1 \\ 0.00001803234135x_1y_1 \\ 0 \end{pmatrix},$$

$$C(x, y, z) = \begin{pmatrix} 8910.35269376x_3y_3z_3 - 0.0006366197723(x_1y_4z_4 + x_4y_1z_4 + x_4y_4z_1) \\ + 0.094954393x_1y_1z_1 - 41.69187427(x_1y_3z_3 + x_3y_1z_3 + x_3y_3z_1) \\ 0.0004300502075x_1y_1z_1 \\ 0.0000004919916745x_1y_1z_1 \\ 0 \end{pmatrix},$$

It is essential to calculate the norms in the center manifold when computing the first Lyapunov coefficient for high-dimensional. There is an invariant expression of the first Lyapunov coefficient:

$$\begin{aligned} l_1(0) &= \frac{1}{2\omega^2} \operatorname{Re} \left(\langle p, C(q, q, \bar{q}) \rangle - 2 \langle p, B(A^{-1}B(q, \bar{q})) \rangle \right. \\ &\quad \left. + \langle p, B(\bar{q}, (2i\omega E - A)^{-1}B(q, q)) \rangle \right) \\ &= -0.2161776 < 0. \end{aligned}$$

Hence H is supercritical Hopf bifurcation, and it branches out the stable limit cycle. Similarly, H_1 is also a supercritical Hopf bifurcation.

3.2. ISIs bifurcation. The more detailed bifurcation caused by direct the current stimulation and k_0 can be described by ISIs series, see Figure.2. As I_{ext} increases in Figure.2(a), the system (2) enters the firing state around $I_{ext} = -0.1964$. Finally, the system (2) terminates the firing state at $I_{ext} \approx 0.7035$. It indicates that Hopf bifurcation and fold bifurcation are the keys to the transition between the quiescent state and the firing state.

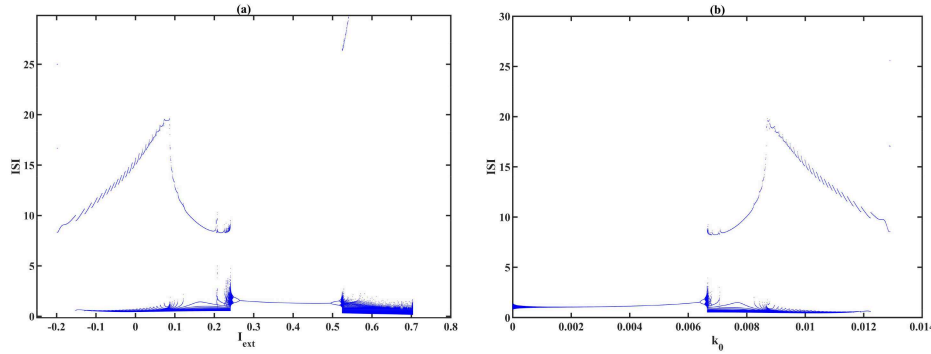


FIGURE 2. (a) The bifurcation diagram of ISIs with respect to I_{ext} .
(b) The bifurcation diagram of ISIs with respect to k_0 .

Moreover, the system presents abundant dynamical properties for $-0.1964 < I_{ext} < 0.7035$. Note that in the Figure.2(a), there are complex dynamic regions around $I_{ext} = 0.0866$, $I_{ext} = 0.2636$ and $I_{ext} = 0.4956$. For $I_{ext} < 0.0866$, there is the period-adding bifurcation. But the period-adding bifurcation terminates, and the maximum value of ISIs changes from increase to decrease around $I_{ext} =$

0.0866. Chaotic bursting is transformed into chaotic spike by inverse period-double bifurcation, and then turns into spike. Then an inverse period-double bifurcation occurs around $I_{ext} = 0.2636$ and leads to chaos. Subsequently, the occurrence of a shrinkage [6] causes the change of bifurcation structure and chaos disappears, which might be caused by a crisis [24]. Similarly, another period-doubling leading to chaos around $I_{ext} = 0.4956$. Here, spike is transformed into chaotic spike caused by period-double bifurcation, and finally become bursting.

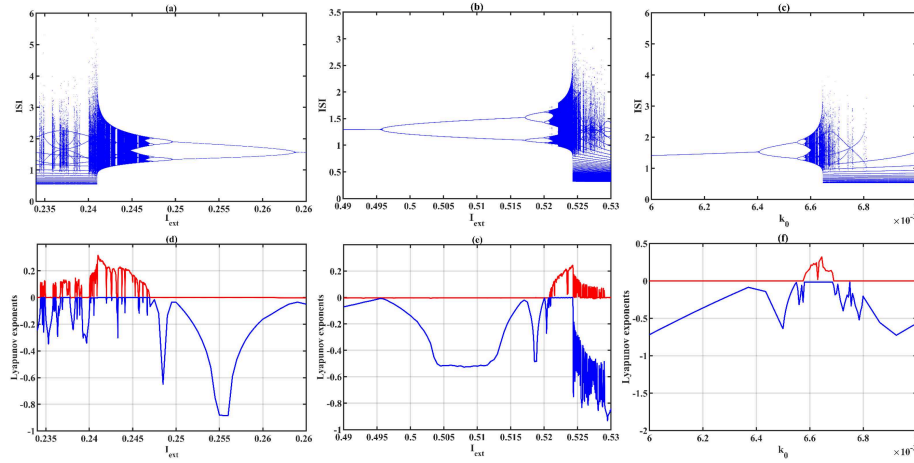


FIGURE 3. (a) The inverse period-double bifurcation of ISIs over the range $[0.234, 0.265]$ of I_{ext} . (b) The period-double bifurcation of ISIs over the range $[0.49, 0.53]$ of I_{ext} . (c) The period-double bifurcation of ISIs over the range $[0.006, 0.007]$ of k_0 . (d), (e), and (f) The first (red) and second (blue) Lyapunov exponents $\lambda_{1,2}$ corresponding to (a), (b), and (c) respectively.

The Lyapunov exponents of the dynamical system is one of the several indicators used to judge whether the dynamical system is chaotic. If the largest Lyapunov exponent is positive and the second Lyapunov exponents is equal to zero, then the system is chaotic. Accordingly, we calculate the first and second Lyapunov exponents to illustrate the chaotic behavior, as shown in Figure.3. Obviously, it is consistent with the behaviors we have described above. Note that, there is a situation that is different from the others. That is, when $I_{ext} > 0.524$, the first Lyapunov exponent is positive, but the second Lyapunov exponent is negative. It can't say this situation is chaotic, since the second Lyapunov exponent is not equal to zero.

The bifurcation diagram of parameter k_0 in Figure.2(b) is similar to the part of bifurcation diagram of parameter I_{ext} . They can generate the same firing modes. It indicates that the feedback current of electromagnetic induction has the same effect on the neuron model as the external forcing currents, and the induced current acts as the external forcing current.

4. Analysis of firing patterns. In this section, we discuss the firing patterns caused by external forcing current and k_0 . Note that, $\rho(\varphi)$ the coupling relation between membrane potential of the neuron and magnetic flux, then we discuss the

effects of strong coupling strength and weak coupling strength on the firing activities of the neuron model.

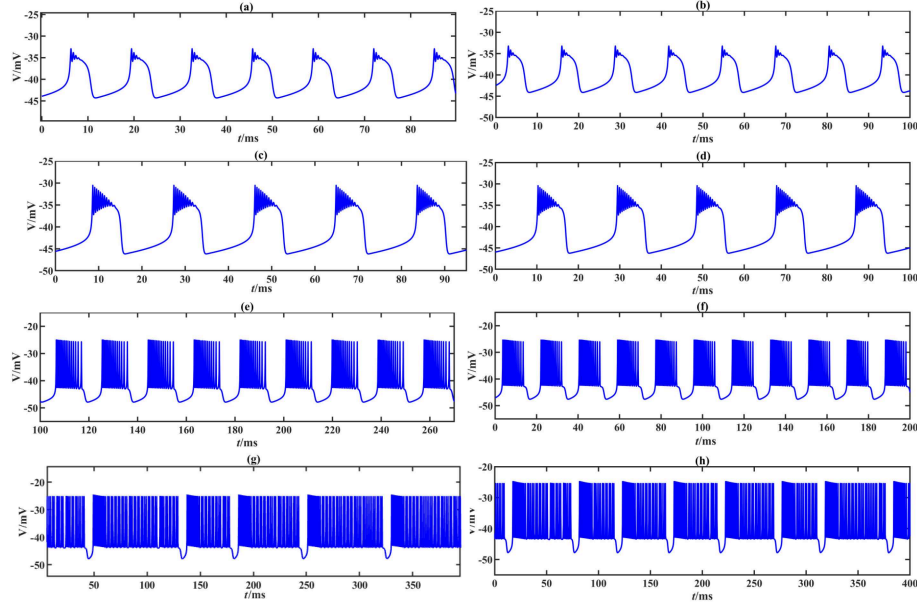


FIGURE 4. The diagrams on the left are the firing patterns generated by I_{ext} , and the diagrams on the right are the firing patterns only produced by induced current. (a) $I_{ext} = -0.1$, (c) $I_{ext} = -0.03$, (e) $I_{ext} = 0.21$, (g) $I_{ext} = 0.2406$, (b) $k_0 = 0.0116$, (d) $k_0 = 0.0104$, (f) $k_0 = 0.0079$, (g) $k_0 = 0.00666$.

4.1. The effect of weak coupling strength. When $\beta = 0.0001$, the feedback of magnetic flux is relatively weak on membrane potential. In this case, there are four bursting patterns, as shown in Figure.4. As can be seen from the Figure.4, the firing patterns caused by the induced current are the same as the firing patterns generated by the external forcing current. In both cases, the neuron model shows regular bursting and spike. We analyze the bursting patterns by using fast-slow dynamics analysis. Since the slow variable c is distinctly slower than the other three variables in the system (2), then we can obtain the fast subsystem:

$$\begin{cases} \frac{dV}{dt} = (-g_{Ca}m_{\infty}^2(V)(V - V_{Ca}) - g_{K(Ca)}s_{\infty}(c)(V - V_K) \\ \quad - g_K n(V - V_K) - k_0 V \rho(\varphi) - I_{ext}) / C_m, \\ \frac{dn}{dt} = (n_{\infty}(V) - n) / \tau_n, \\ \frac{d\varphi}{dt} = -f_c (\theta g_{Ca}m_{\infty}^2(V)(V - V_{Ca}) + k_{PMCAc}), \end{cases} \quad (6)$$

and the slow subsystem:

$$\frac{dc}{dt} = -f_c (\theta g_{Ca}m_{\infty}^2(V)(V - V_{Ca}) + k_{PMCAc}), \quad (7)$$

Thus, we treat slow variable c as a bifurcation parameter of the fast subsystem (6), then, we get four bursting types according to the bifurcation of the transition between the quiescent and firing state through numerical calculations. We present the numerical results of bifurcation analysis of the fast subsystem (6) by using MATCONT software.

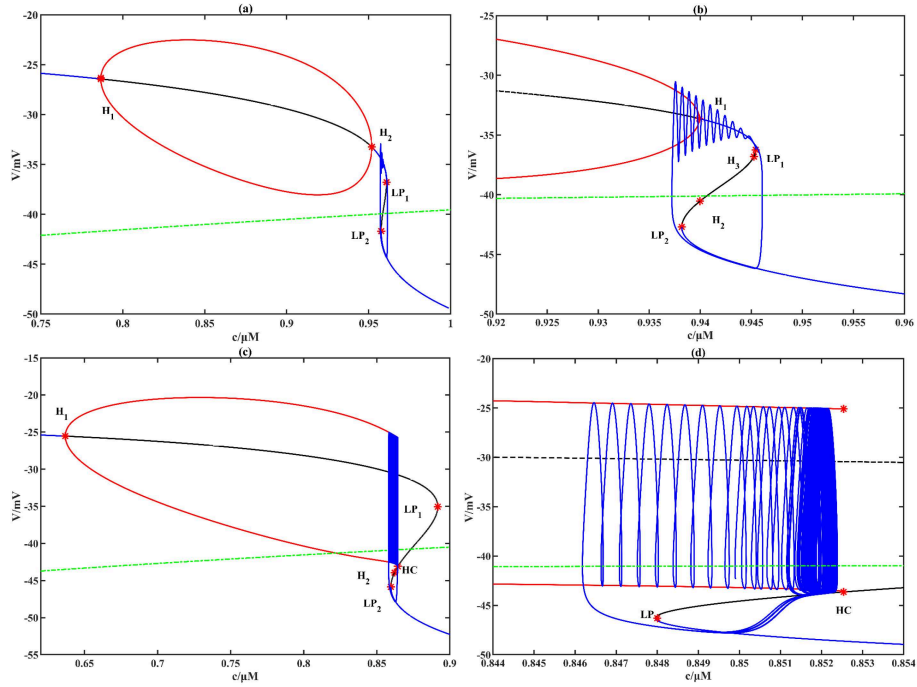


FIGURE 5. The fast-slow analysis of fast subsystem under different external forcing currents. The dotted green curve is slow-nullcline for $\dot{c} = 0$, the black and blue lines are stable and unstable equilibria. The trajectory of the system (2) (the blue curve) is superimposed. (a) $I_{ext} = -0.1$, (b) $I_{ext} = -0.03$, (c) $I_{ext} = 0.21$, (d) $I_{ext} = 0.2406$.

4.1.1. “Fold/fold” bursting via the “point-point” hysteresis loop. For $I_{ext} = -0.1$, we draw the bifurcation diagram of the fast subsystem with respect to the slow variable, as shown in Figure.5(a). The bifurcation curve of the fast subsystem presents Z-shape. The stable equilibria lose stability via H_1 , and branch a stable limit cycle. Then the unstable equilibria transform into stable via H_2 , and the stable limit cycle vanishes. Note that, with the decrease of the slow variable, the lower quiescence state disappears via fold bifurcation LP_2 on the invariant circle (SNIC), and the trajectory doesn’t pass through the stable limit cycle corresponding to the firing state. After that, the trajectory attenuation oscillates to another fold bifurcation LP_1 , and then jumps into the lower quiescent state. Thus, the bursting process is completed and starts another. Since the trajectory doesn’t cross the limit cycle attractor, then we only consider the bifurcation generated by the hysteresis loop. According to the classification of bursting types [8], this bursting type belongs to the “fold/fold” hysteresis loop bursting of point-point type.

4.1.2. *“Fold/Hopf” bursting via the “fold/fold” hysteresis loop.* When $I_{ext} = -0.03$, the second bursting pattern is shown in Figure.5(b). The bifurcation curve of the fast subsystem with respect to slow variable c is also a Z-shape curve, and the upper and lower branch of Z-shape curve intersects with the middle branch forming the fold bifurcation point LP_i ($i = 1, 2$). Equally, there are two Hopf bifurcation points (The left-hand is not drawn) and the limit cycle is located between Hopf bifurcation points. Now we analyze the generating process of bursting through Figure.5(b). The quiescent state vanishes via fold bifurcation LP_2 , and switches to the firing state corresponding to the limit cycle attractor. Then c begins to decrease and the trajectory crosses the Hopf bifurcation point H_1 indicating the system ends the firing state. Finally, the trajectory jumps into the lower quiescent state via LP_2 . Hence the bifurcation of transformation between quiescent and firing state is “fold/Hopf” type bursting, and the bifurcation of the hysteresis loop is “fold/fold” type. Therefore, the model presents “fold/Hopf” bursting via the “fold/fold” hysteresis loop.

4.1.3. *“Fold/homoclinic” bursting via the “fold/homoclinic” hysteresis loop.* Now we analyze the third type of bursting of the system (2). There are regular and chaotic bursting of this type for different I_{ext} .

When $I_{ext} = 0.21$, the model exhibits the “fold/homoclinic” regular bursting. As shown in Figure.5(c), the limit cycle of the upper branch of the Z-shape bifurcation curve intersects with the middle branch of the Z-shape curve forming a saddle homoclinic orbit. According to the trajectory superimposed on Figure.5(c), the model switches to the firing state through fold bifurcation LP_2 , then the repetitive spiking oscillates near to the saddle homoclinic orbit, so the firing state disappears via saddle homoclinic bifurcation. We can see the same bifurcation form the hysteresis loop. Therefore, the model exhibits “fold/homoclinic” bursting via the “fold/homoclinic” hysteresis loop.

Moreover, we also obtain the chaotic bursting of the model for $I_{ext} = 0.2406$, where the largest Lyapunov exponent is positive, and the chaotic behavior is shown by fast-slow dynamics analysis in Figure.5(d). We find that the model enters the repetitive spiking state, when the trajectory is closed to saddle homoclinic bifurcation. After a while, the model terminates the spiking state via the saddle homoclinic orbit. So, the bifurcation of transformation between the firing and quiescent and hysteresis loop is the same as $I_{ext} = 0.21$. Thus, it is “fold/homoclinic” chaotic bursting via the “fold/homoclinic” hysteresis loop.

4.1.4. *“SubHopf/homoclinic” bursting via the “fold/homoclinic” hysteresis loop.* Interestingly, by changing parameter, the model can also exhibit the intrinsic pseudo-plateau bursting, which is very common in endocrine model, as shown in Figure.6.

In Figure.6(b), the quiescent state vanishes via fold bifurcation LP_2 . Then, the trajectory starts to oscillate around the stable equilibrium on the upper branch, soon afterward the trajectory crosses the subcritical Hopf bifurcation point entering the spiking state. At last, the spiking state disappears through a homoclinic orbit and shifts to the lower branch corresponding to the quiescence state. Thus, this electrical activity of the model is called “subHopf/homoclinic” bursting via the “fold/homoclinic” hysteresis loop.

4.2. **The effect of strong coupling strength.** Now we consider increase the feedback of the magnetic flux on the membrane potential, and set $\beta = 0.001$ and $k_2 = 2.5$. Firstly, electrical activities of the neuron model show the firing rhythm

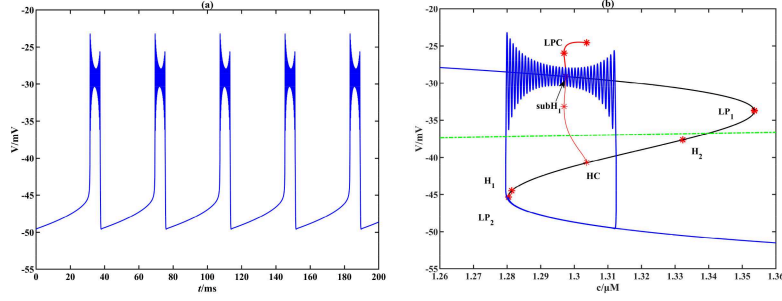


FIGURE 6. The diagram of the membrane potential sequence for $I_{ext} = -0.5$, $V_{ml} = -27.5$. (b) Fast-slow dynamics of “subHopf/homoclinic” bursting via the “fold/homoclinic” hysteresis loop. The point $subH_1$ represent subcritical Hopf bifurcation. H_i are neutral saddle, LP_i represent fold bifurcation. HC represents the saddle homoclinic bifurcation. LPC is the limit point of cycle.

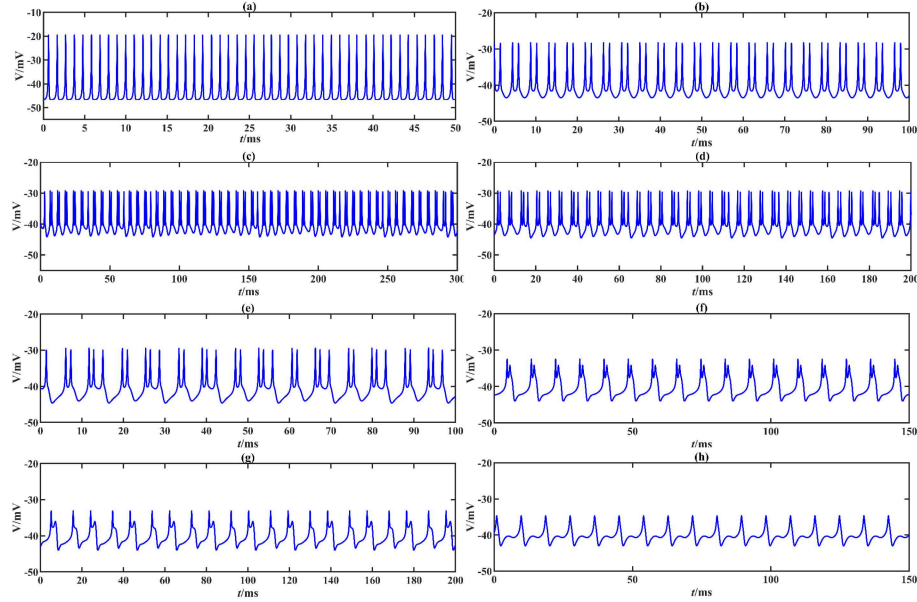


FIGURE 7. Firing patterns of neuron model with variations of k_0 . (a) $k_0 = 0.0001$, (b) $k_0 = 0.007$, (c) $k_0 = 0.007408$ (d) $I_{ext} = 0.00742$ (e) $k_0 = 0.00747$, (f) $k_0 = 0.0085$, (g) $k_0 = 0.00866$, (h) $k_0 = 0.009$.

only caused by electromagnetic radiation is different from above, and numerical results are shown in Figure.7. When the induced current is small, the neuron presents spike state. With the increase of parameter k_0 , the firing pattern of the neuron changes into a period-2 pattern, while the neuron model enters into mixed

bursting when k_0 increase to 0.007408. For higher k_0 , the neuron model presents subthreshold oscillations and quiescent state.

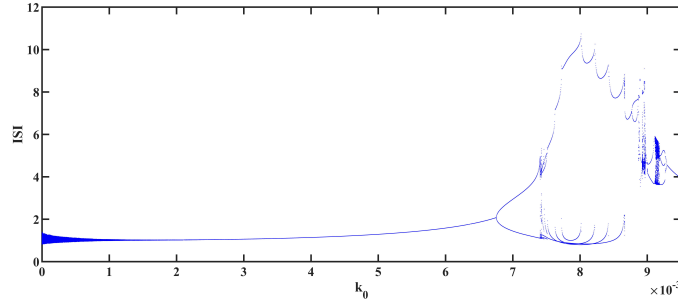


FIGURE 8. ISIs bifurcation diagram with respect to k_0 , $I_{ext}=0$.

When the combined effects of induced current and the external forcing currents are considered, the electrical activities of neuron model become more abundant. As shown in Figure.10 and Figure.12, ISIs bifurcation diagram is more complex. By changing the parameters I_{ext} , the neuron model can select different firing modes by applying external forcing current under induced current of different intensity in Figure.9 and Figure.11. The firing activities show that system fires with subthreshold oscillations, regular bursting, and mixed bursting for $k_0 = 0.01$. While increasing the intensity of induced current, the neuron model presents subthreshold oscillations and MMOs for $k_0 = 0.02$. Note that the regular mixed-mode oscillations alternate with the irregular mixed-mode oscillations, as shown in Figure.11 (b) and (c). Therefore, with the increase of induced current, the response of the neuron model to the stimulus current changes from bursting pattern to MMOs. It indicates that the firing behaviors of the neuron model can be regulated by both induced current and direct current stimulation.

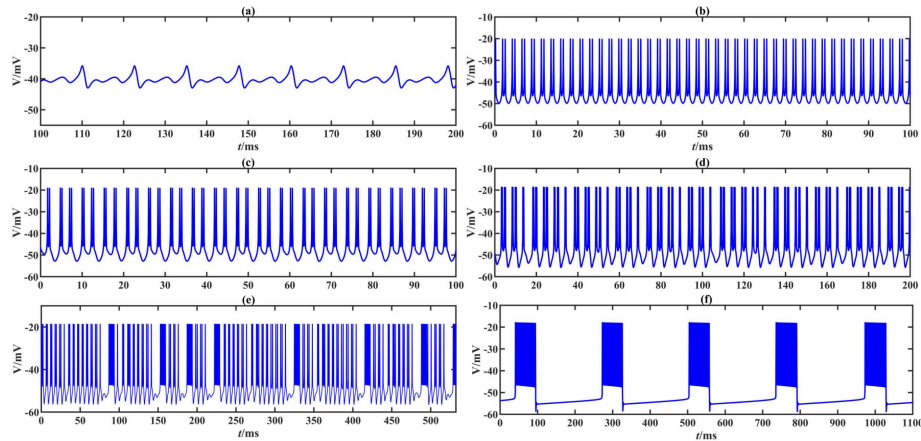
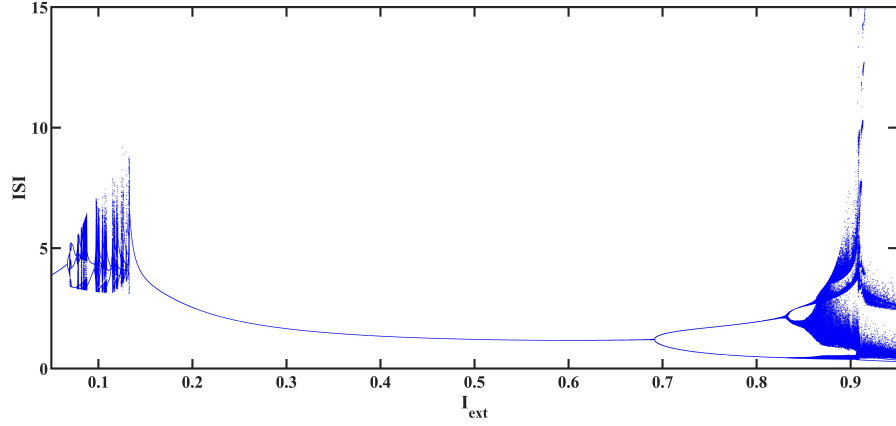
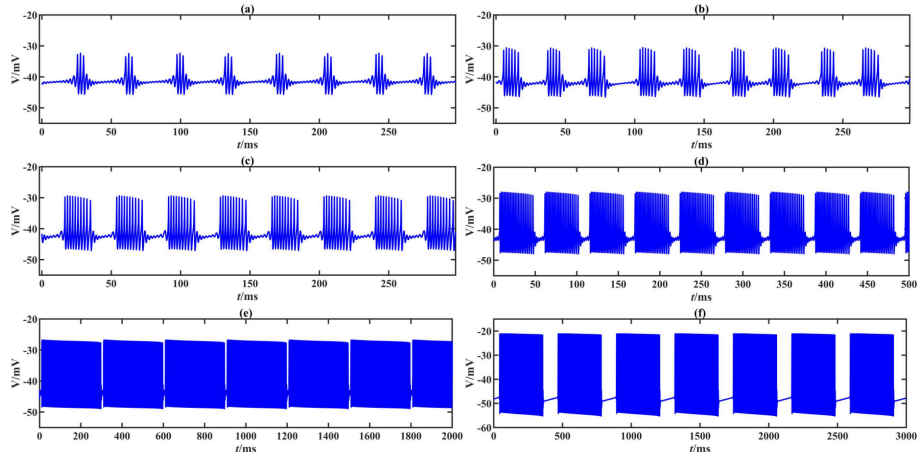


FIGURE 9. Firing patterns of neuron model with variations of I_{ext} , $k_0 = 0.01$. (a) $I_{ext} = 0.075$, (b) $I_{ext} = 0.75$, (c) $I_{ext} = 0.85$, (d) $I_{ext} = 0.895$, (e) $I_{ext} = 0.9075$, (f) $I_{ext} = 0.95$.

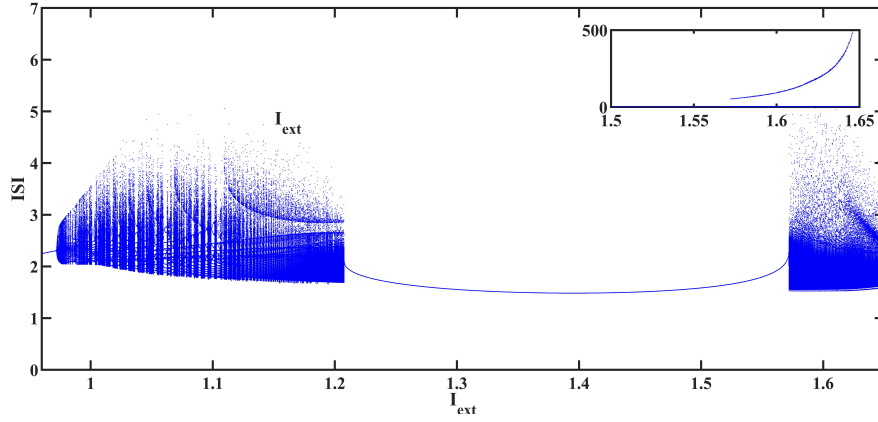
FIGURE 10. ISIs bifurcation diagram with respect to I_{ext} , $k_0=0.01$.FIGURE 11. Firing patterns of neuron model with variations of I_{ext} , $k_0 = 0.02$. (a) $I_{ext} = 1$, (b) $I_{ext} = 1.04$, (c) $I_{ext} = 1.08$, (d) $I_{ext} = 1.14$, (e) $I_{ext} = 1.2$, (f) $I_{ext} = 1.6$.

5. Codimension-two bifurcation analysis. In this section, we use the bifurcation theory of dynamical systems and numerical simulation to investigate the codimension-two bifurcation in the improved neuron model in (I_{ext}, k_0) phase plane and other parameters are given in Table 1.

5.1. Bifurcation in (I_{ext}, k_0) -plane. The existence of stable limit cycles indicates that the neuron model will present firing activities, such as spike or bursting. The region of oscillation activities can be detected by two-parameter bifurcation analysis, as shown in Figure.13. The region of oscillation activities roughly locates in the region surrounded by Hopf bifurcation curve h_1 in Figure.13(b). For fixed k_0 , the bifurcation of the transformation between the quiescent state and the firing state is related to the boundaries of the region surrounded by h_1 . For example, when $k_0 = 0.03$, the boundary points are Hopf bifurcation points. It means that

TABLE 2. Data related to special points

Poins	Parameter values (I_{ext}, k_0)	Eigenvalues ($\lambda_1, \lambda_2, \lambda_3, \lambda_4$)	Normal Form Parameter
CP_1	(-64.649,-12.888)	$\lambda_1 = 0, \lambda_2 = -19.1961,$ $\lambda_3 = -3.0007, \lambda_4 = 3447$	$c = -4.21 \times 10^{-4}$
CP_2	(-66.356,-1.1266)	$\lambda_1 = 0, \lambda_2 = -88.818 + 206.79i$ $\lambda_3 = -88.818 - 206.79i, \lambda_4 = -2.999,$	$c = -3.22 \times 10^{-4}$
CP_3	(-78.42135,-4.6267)	$\lambda_1 = 0, \lambda_2 = -2.9873,$ $\lambda_3 = 4.4263, \lambda_4 = 1.003963$	$c = 1.9 \times 10^{-4}$
CP_4	(-23.9617,-0.5826)	$\lambda_1 = 0, \lambda_2 = -29.6947,$ $\lambda_3 = 193.632, \lambda_4 = -3.0969$	$c = -2.33 \times 10^{-5}$
CP_5	(-16.1428,0.3545)	$\lambda_1 = 0, \lambda_2 = -14.6374,$ $\lambda_3 = -3.1904, \lambda_4 = 90.4468$	$c = 3.66 \times 10^{-5}$
CP_6	(1.599659,0.025901)	$\lambda_1 = 0, \lambda_2 = -30.6756,$ $\lambda_3 = -2.71, \lambda_4 = 2.0821$	$c = 9.29 \times 10^{-5}$
GH_1	(-5.514,-0.07359)	$\lambda_1 = 1.0119i, \lambda_2 = -1.0119i,$ $\lambda_3 = -3.73 + 4.19i, \lambda_4 = -3.73 - 4.19i$	$l_1 = 36, 03$
GH_2	(-13.993,-0.22718)	$\lambda_1 = 70.688i, \lambda_2 = -70.6880i,$ $\lambda_3 = -2.98418654, \lambda_4 = -0.00208283$	$l_1 = -1.7 \times 10^{-3}$
GH_3	(1.98293,0.33597)	$\lambda_1 = 0.09056i, \lambda_2 = -0.09056i,$ $\lambda_3 = -30.013089, \lambda_4 = -2.371837$	$l_1 = -0.117$
GH_4	(-7.88796,-0.10746)	$\lambda_1 = 20.5112i, \lambda_2 = -20.5112i,$ $\lambda_3 = -2.8259, \lambda_4 = -0.016958$	$l_1 = -7.8 \times 10^{-3}$
GH_5	(-7.7194,-0.1145)	$\lambda_1 = 2.35556i, \lambda_2 = -2.35556,$ $\lambda_3 = 0.715 + 1.936i, \lambda_4 = 0.715 - 1.936i$	$l_1 = -2.5 \times 10^5$
GH_6	(-7.68801,-0.11345)	$\lambda_1 = 1.577914i, \lambda_2 = -1.577914i,$ $\lambda_3 = 0.582 + 3.039i, \lambda_4 = 0.582 - 3.039i$	$l_1 = -4.4 \times 10^6$
GH_7	(-67.9198,-1.7171)	$\lambda_1 = 214.4301i, \lambda_2 = -214.4301i,$ $\lambda_3 = -2.999953, \lambda_4 = -0.000808023$	$l_1 = -0.03122$
GH_8	(-67.1444,-1.6382)	$\lambda_1 = 206.6605i, \lambda_2 = -206.6605i,$ $\lambda_3 = -2.9997, \lambda_4 = -0.00073251$	$l_1 = 0.03811$
GH_{10}	(-64.649,-12.888)	$\lambda_1 = 1.268 \times 10^{-7}i, \lambda_2 = -1.268 \times 10^{-7}i,$ $\lambda_3 = 2.999109, \lambda_4 = 1394.19249$	$l_1 = 8.63 \times 10^{-3}$
ZH_1	(-73.3066,-6.1271)	$\lambda_1 = 209.65718i, \lambda_2 = -209.65718i,$ $\lambda_3 = 0, \lambda_4 = -2.99981307$	$(s, \theta, E_0) =$ $(1, -5866.3, -1)$
ZH_2	(-67.4984,-1.6958)	$\lambda_1 = 212.9485i, \lambda_2 = -212.9485i,$ $\lambda_3 = 0, \lambda_4 = 2.999916$	$(s, \theta, E_0) =$ $(-1, 4043.5, -1)$
BT_1	(-73.124,-6.294215)	$\lambda_1 = 0, \lambda_2 = 0,$ $\lambda_3 = -3, \lambda_4 = 1420.03$	$a = 1.19 \times 10^{-3}$ $b = 1.097$
BT_2	(0.64939,0.00913)	$\lambda_1 = 0, \lambda_2 = 0,$ $\lambda_3 = -33.0915, \lambda_4 = -2.7655$	$a = 4.54 \times 10^{-4}$ $b = 0.455$
BT_3	(-47.737,1.87268)	$\lambda_1 = 0, \lambda_2 = 0,$ $\lambda_3 = -2.7509, \lambda_4 = 416.481$	$a = 6.1 \times 10^{-3}$ $b = 6.147$
HH_1	(-7.4232,-0.10856)	$\lambda_1 = 3.700106i, \lambda_2 = -3.700106i,$ $\lambda_3 = 1.3485054i, \lambda_4 = -1.3485054i$	$(p_{11}p_{22}, \vartheta, \delta) =$ $(1, -2, -2)$ $(\Theta, \Delta) =$ $(-50.2, 285)$
NS_1	(-72.904,-5.822)	$\lambda_1 = 0, \lambda_2 = 1285.27,$ $\lambda_3 = -3, \lambda_4 = 3$	None
NS_2	(-1.3217,-0.03665)	$\lambda_1 = 0, \lambda_2 = -3.054,$ $\lambda_3 = -29.495, \lambda_4 = 29.495$	None
NS_3	(1.5887,0.02568)	$\lambda_1 = 0, \lambda_2 = -30.46293,$ $\lambda_3 = -2.74899, \lambda_4 = 2.74899$	None

FIGURE 12. ISIs bifurcation diagram with respect to I_{ext} , $k_0=0.02$.

the bifurcation of the transformation between the quiescent state and the firing state is Hopf bifurcation. While $k_0 = 0.01$, the bifurcation is fold bifurcation and Hopf bifurcation.

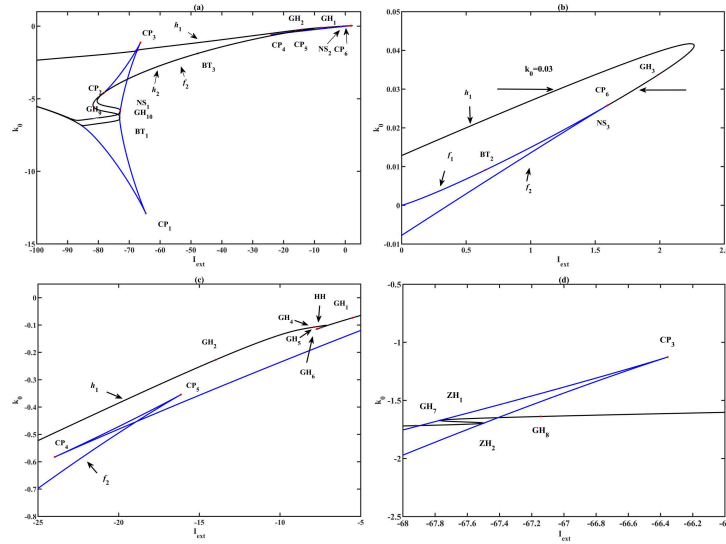


FIGURE 13. Codimension-two bifurcation analysis of the neuron model. (a) Representation of the two-parameter bifurcation diagram in the (I_{ext}, k_0) -plane. (b)-(d) are the partial enlargements of the diagram (a). f_1 and f_2 are the fold bifurcation curves; h_1 and h_2 are Hopf bifurcation curves.

We use MATCONT software to calculate codimension-two bifurcation points. The meaning of each label in the figure is interpreted as follows: CP_i ($i = 1, \dots, 6$) are the cusp bifurcation; BT_i ($i = 1, 2, 3$) represent Bogdanov-Takens bifurcation; ZH_i ($i = 1, 2$) indicate fold-Hopf bifurcation; GH_i ($i = 1, \dots, 10$) represent Bautin

bifurcation; HH is Hopf-Hopf bifurcation; NS_i ($i = 1, 2, 3$) are neutral saddle. Readers can refer to [10] for understanding the meaning of this bifurcation points. The more detailed data is shown in Table 2.

From Figure.13 (a) and (b), we can see that the fold bifurcation curve f_1 and Hopf bifurcation curve h_1 seem to be coincident into one curve, and two curves are tangent at BT_2 . It indicates that the equilibrium and eigenvalue change greatly, even if the parameter value changes slightly. The same situation occurs between the curves f_2 and h_2 , and they are tangent at BT_3 . Moreover, most of the codimension-two bifurcation points occur on h_1 and f_2 .

For cusp points CP_i , the system (2) has a zero eigenvalue. Especially, near each CP_i , the system (2) is locally topologically equivalent to the following normal form:

$$\begin{cases} \dot{\eta} = \beta_1 + \beta_2\eta + s\eta^3, \\ \dot{\xi}_- = -\xi_-, \\ \dot{\xi}_+ = \xi_+, \end{cases} \quad (8)$$

where $\xi_{\pm} \in \mathbf{R}^1$, \mathbf{R}^2 , $\beta_{1,2} \in \mathbf{R}$

$$s = \text{sign}(c) = \begin{cases} 1 & \text{for } CP_i, i = 1, 2, 4 \\ -1 & \text{for } CP_i, i = 3, 5, 6 \end{cases}$$

There are three Bogdanov-Takens bifurcations labeled BT_i ($i = 1, 2, 3$) with two eigenvalues $\lambda_{1,2} = 0$. Bogdanov-Takens bifurcation is the tangency point of the Hopf bifurcation curve and fold bifurcation curve. Near the point BT_i , the system can be simplified as the following topological normal form:

$$\begin{cases} \frac{d\eta_1}{dt} = \eta_2, \\ \frac{d\eta_2}{dt} = \beta_1 + \beta_2\eta_1 + \eta_1^2 + s\eta_1\eta_2, \end{cases} \quad (9)$$

where $\beta_1, \beta_2 \in \mathbf{R}$, $s = \text{sign}(ab) = 1$.

There are ten generalized Hopf bifurcation points. We know Bautin bifurcation is the degenerated Hopf bifurcation whose first Lyapunov coefficient is equal to zero. Near the Bautin bifurcation points GH_i ($i = 1, \dots, 4, 6, \dots, 10$), the differential system is equivalent to the following topological normal form:

$$\begin{cases} \dot{z} = (\beta_1 + i)z + \beta_2z|z|^2 + sz|z|^4, & z \in \mathbf{C}^1 \\ \dot{\xi}_{\pm} = \pm \xi_{\pm}, & \xi_{\pm} \in \mathbf{R}^2 \end{cases} \quad (10)$$

where $\beta_1, \beta_2 \in \mathbf{R}$, when real eigenvalue is positive, $\dot{\xi}_+ = \xi_+$, otherwise $\dot{\xi}_- = \xi_-$,

$$s = \text{sign}(l_2) = \begin{cases} 1, & i = 1, 8, 10, \\ -1, & i = 2, 3, 4, 6, 7, 9, \end{cases}$$

Near the bifurcation point GH_5 , the differential system is equivalent to the following topological normal form:

$$\begin{cases} \dot{z} = (\beta_1 + i)z + \beta_2z|z|^2 + sz|z|^4, & z \in \mathbf{C}^1 \\ \dot{\xi}_+ = \xi_+, & \xi_+ \in \mathbf{R} \\ \dot{\xi}_- = -\xi_-, & \xi_- \in \mathbf{R} \end{cases} \quad (11)$$

where $\beta_1, \beta_2 \in \mathbf{R}$, $s = \text{sign}(l_2) = -1$.

Further, there are two fold-Hopf bifurcation points, their eigenvalues consist of one zero eigenvalue, a pair of purely imaginary eigenvalues, and one nonzero real eigenvalue, but they don't have the fixed normal form. A Hopf-Hopf bifurcation labeled HH occurs, and it has two pairs of purely imaginary eigenvalues, but it has no fixed normal form like the fold-Hopf bifurcation. The meaning of NS_i ($i = 1, 2, 3$) are zero-neutral saddle with one zero eigenvalue and two real eigenvalues that satisfy their sum is equal to zero.

5.2. Bogdanov-Takens bifurcation analysis. In this section, we investigate the Bogdanov-Takens bifurcation of the system (2) through the method proposed by [3]. We treat (I_{ext}, k_0) as a pair of bifurcation parameters, other parameters are given by Table 1. We select BT_2 as the point of analysis, where $(I_{ext}, k_0) = (0.649385813300958, 0.00912704116143242) = \mu_0$, and its coordinate is $(V, n, c, \varphi) = (-60.0447105, 0.0005496996, 0.07053964, -20.014904) = x_0$. Now we can rewrite the system (2) as the following:

$$\frac{dx}{dt} = F(x, \mu) = \begin{pmatrix} F_1(x, \mu) \\ F_2(x, \mu) \\ F_3(x, \mu) \\ F_4(x, \mu) \end{pmatrix}, \quad (12)$$

where $x = (V, n, c, \varphi)$, $\mu = (I_{ext}, k_0)$, and

$$\begin{cases} F_1(x, \mu) = (-g_{Ca}m_{\infty}^2(V)(V - V_{Ca}) - g_{K(Ca)}s_{\infty}(c)(V - V_K) \\ \quad - g_K n(V - V_K) - k_0 V \rho(\varphi) - I_{ext}) / C_m, \\ F_2(x, \mu) = (n_{\infty}(V) - n) / \tau_n, \\ F_3(x, \mu) = -f_c(\theta g_{Ca}m_{\infty}^2(V)(V - V_{Ca}) + k_{PMCAc}), \\ F_4(x, \mu) = k_1 V - k_2 \varphi, \end{cases} \quad (13)$$

where m_{∞} , s_{∞} , n_{∞} , $\rho(\varphi)$ are the same as before.

Afterward, we can obtain the Taylor series of $F(x, \mu)$ around (x_0, μ_0) as the following:

$$\begin{aligned} F(x, \mu) = & DF(x_0, \mu_0)(x - x_0) + F_{\mu}(x_0, \mu_0)(\mu - \mu_0) \\ & + \frac{1}{2} D^2 F(x_0, \mu_0)(x - x_0, x - x_0) + F_{\mu x}(x - x_0, \mu - \mu_0) + \cdots, \end{aligned}$$

Note

$$\begin{aligned} B = & DF(x - x_0) \\ = & \begin{pmatrix} 0.478318902499 & -3548.964657 & -0.181409523688 & -0.698294125384 \\ 0.002289155829 & -33.3333333 & 0 & 0 \\ 0.000020177552 & 0 & -0.002 & 0 \\ 1 & 0 & 0 & -3 \end{pmatrix}, \end{aligned}$$

Then we can get the eigenvalues of matrix B , specifically, 0, 0, -33.09149, -2.765521.

Let $P = (p_1, p_2, P_0)$ be an invertible matrix, which satisfies $P^{-1}AP = \begin{pmatrix} J_0 & 0 \\ 0 & J_1 \end{pmatrix}$,

where $J_0 = \begin{pmatrix} 0 & 1 \\ 0 & 0 \end{pmatrix}$, $J_1 = \begin{pmatrix} -33.0914934 & 0 \\ 0 & -2.765521027 \end{pmatrix}$, p_1, p_2 are the generalized eigenvectors of matrix B corresponding to the double-zero eigenvalue and P_0 consists of the generalized eigenvectors of the matrix J_1 .

So, we can get

$$\begin{aligned} p_1 &= (1, 0.00006867467488, 0.01008877620911, 0.3333333333)^T, \\ p_2 &= (1, 0.00006661443401, -5.0342993201, 0.2222222222)^T, \\ P_0 &= \begin{pmatrix} -0.9994035531, & -0.009459936886, & 0.000000609423581, & 0.03321216198 \\ -0.2282872781, & -0.00001709592915, & 0.000001666815078, & -0.9735938159 \end{pmatrix}^T, \end{aligned}$$

We define $P^{-1} = (q_1, q_2, Q_0)^T$, then

$$\begin{aligned} q_1 &= (1.090466731, -116.0938562, 0.2038746394, -0.2536526072)^T, \\ q_2 &= (0.002185428812, -0.2326802884, -0.1982288, -0.0005086907003)^T, \\ Q_0 &= \begin{pmatrix} 0.007255602957, & -106.47488401, & 0.0000397780618, & 0.0001683713352 \\ 0.3740939287, & -43.43281481, & 0.02455715043, & -1.114076838 \end{pmatrix}^T. \end{aligned}$$

According to expression (28) and (29) in [3], we can obtain

$$\begin{aligned} a &= \frac{1}{2} p_1^T (q_2 \cdot D^2 F(x_0, \mu_0)) p_1 = 4.537776612 \times 10^{-4}, \\ b &= p_1^T (q_1 \cdot D^2 F(x_0, \mu_0)) p_1 + p_1^T (q_2 \cdot D^2 F(x_0, \mu_0)) p_2 = 0.4552873824, \end{aligned}$$

$$\begin{aligned} S_1 &= F_\mu^T(x_0, \mu_0) q_2 = (-0.6956435964, 43.44299811)^T, \\ S_2 &= \left[\frac{2a}{b} (p_1^T (q_1 \cdot D^2 F(x_0, \mu_0)) p_2 + p_2^T (q_2 \cdot D^2 F(x_0, \mu_0)) p_2) \right. \\ &\quad \left. - p_1^T (q_2 \cdot D^2 F(x_0, \mu_0)) p_2 \right] F_\mu^T(x_0, \mu_0) q_1 \\ &\quad + \left(q_2 \cdot \left(F_{\mu X}(x_0, \mu_0) - ((P_0 J_1^{-1} Q_0) F_\mu(x_0, \mu_0))^T D^2 F(x_0, \mu_0) \right) \right) p_1 \\ &\quad - \frac{2a}{b} \sum_{i=1}^2 \left(q_i \cdot \left(F_{\mu x}(x_0, \mu_0) - ((P_0 J_1^{-1} Q_0) F_\mu(x_0, \mu_0))^T D^2 F(x_0, \mu_0) \right) \right) p_i \\ &= (0.2983460742, -18.6344014)^T \end{aligned}$$

Let $\lambda_1 = I_{ext} - 0.64939$ and $\lambda_2 = k_0 - 0.009127$, then we treat λ_1, λ_2 as a pair of bifurcation parameters. Thus, we have

$$\begin{aligned} \beta_1 &= S_1^T (\mu - \mu_0) = -0.6956435964\lambda_1 + 43.44299811\lambda_2, \\ \beta_2 &= S_2^T (\mu - \mu_0) = 0.2983460741\lambda_1 - 18.63440137\lambda_2, \end{aligned}$$

By using Theorem 1 in [3], the system (12) at $x = x_0, \mu = \mu_0$ is locally topologically equivalent to

$$\begin{cases} \frac{dz_1}{dt} = z_2, \\ \frac{dz_2}{dt} = \beta_1 + \beta_2 z_1 + a z_1^2 + b z_1 z_2, \\ \quad = -0.6956435964\lambda_1 + 43.442998\lambda_2 + (0.298346074\lambda_1 - 18.6344014\lambda_2) z_1, \\ \quad + 0.0004537776612 z_1^2 + 0.4552873824 z_1 z_2, \end{cases} \quad (14)$$

Moreover, we can transform the variables by

$$\begin{aligned} t &= \left| \frac{b}{a} \right| = \left| \frac{0.4552873824}{4.537776612 \times 10^{-4}} \right| t_1, \\ z_1 &= \frac{a}{b^2} \eta_1 = \frac{4.537776612 \times 10^{-4}}{0.4552873824^2} \eta_1, \\ z_2 &= \operatorname{sign} \left(\frac{b}{a} \right) \frac{a^2}{b^3} \eta_2 = \frac{0.0004537776612^2}{0.4552873824^3} \eta_2. \end{aligned}$$

Then system (12) is transformed into the following:

$$\begin{cases} \frac{d\eta_1}{dt} = \eta_2, \\ \frac{d\eta_2}{dt} = \bar{\beta}_1 + \bar{\beta}_2 \eta_1 + \eta_1^2 + s\eta_1 \eta_2, \end{cases} \quad (15)$$

where

$$\begin{aligned} \bar{\beta}_1 &= \frac{b^4}{a^3} \beta_1 = -3.1988944710853 \times 10^8 \lambda_1 + 1.997712149909 \times 10^{10} \lambda_2, \\ \bar{\beta}_2 &= \frac{b^2}{a^2} \beta_2 = 3.003345752 \times 10^5 \lambda_1 - 1.875860118 \times 10^7 \lambda_2. \end{aligned}$$

By the theory in [10], we can compute the following terms:

$$\begin{aligned} 4\bar{\beta}_1 - \bar{\beta}_2^2 &= 0 \Leftrightarrow -70.49377359\lambda_1^2 + 8805.943066\lambda_1\lambda_2 \\ &\quad - 275005.2569\lambda_2^2 - \lambda_1 + 62.4500798\lambda_2 = 0, \\ \bar{\beta}_1 &= 0 \Leftrightarrow \lambda_1 = 62.45007979995\lambda_2, \\ \bar{\beta}_2 &< 0 \Leftrightarrow \lambda_1 = 62.45901315873\lambda_2, \\ \bar{\beta}_1 + \frac{6}{25}\bar{\beta}_2^2 &= o(\bar{\beta}_2^2) \Leftrightarrow 2.1648206 \times 10^{10}\lambda_1^2 - 2.70425113 \times 10^{12}\lambda_1\lambda_2 \\ &\quad - 3.19889447 \times 10^8\lambda_1 + 8.44524284 \times 10^{13}\lambda_2^2 \\ &\quad + 1.9977121499 \times 10^{10}\lambda_2 = o(\|\lambda_1, \lambda_2\|^2). \end{aligned}$$

According to the theory in [10] and our results of calculation, we have the following:

Theorem 5.1. *Let (I_{ext}, k_0) be the Bogdanov-Takens bifurcation point of systems (12). Denote $\bar{\lambda}_1 = I_{ext} - 0.64939$, $\bar{\lambda}_2 = k_0 - 0.009127$. Then if $0 < \|\bar{\lambda}_1, \bar{\lambda}_2\|^2 \ll 1$, the dynamics on the center manifold of the system (12) near $x = x_0$, $\mu \approx \mu_0$ is locally topologically equivalent to the following system:*

$$\begin{cases} \frac{d\eta_1}{dt} = \eta_2, \\ \frac{d\eta_2}{dt} = 3.19889447 \times 10^8 \bar{\lambda}_1 + 1.9977121499 \times 10^{10} \bar{\lambda}_2 + \eta_1^2 \\ \quad + (3.003345752 \times 10^5 \bar{\lambda}_1 - 1.875860118 \times 10^7 \bar{\lambda}_2) \eta_1 + s\eta_1 \eta_2, \end{cases} \quad (16)$$

In addition, system (16) has three bifurcation curves in the small neighborhood near the origin:

(i) there is a saddle-node bifurcation curve:

$$\begin{aligned} SN = \{(\bar{\lambda}_1, \bar{\lambda}_2) : &-70.49377359\bar{\lambda}_1^2 + 8805.943066\bar{\lambda}_1\bar{\lambda}_2 - 275005.2569\bar{\lambda}_2^2 \\ &- \bar{\lambda}_1 + 62.45007979995\bar{\lambda}_2 = 0\}; \end{aligned}$$

(ii) there exists a Hopf bifurcation curve:

$$H = \{(\bar{\lambda}_1, \bar{\lambda}_2) : \bar{\lambda}_1 = 62.45901315873076\bar{\lambda}_2, \bar{\lambda}_2 < 0\};$$

(iii) there exists a saddle homoclinic bifurcation curve:

$$\begin{aligned} HC = & \{(\bar{\lambda}_1, \bar{\lambda}_2) : 2.1648206 \times 10^{10} \bar{\lambda}_1^2 - 2.70425113 \times 10^{12} \bar{\lambda}_1 \bar{\lambda}_2 \\ & - 3.19889447 \times 10^8 \bar{\lambda}_1 + 8.44524284 \times 10^{13} \bar{\lambda}_2^2 + 1.9977121499 \times 10^{10} \bar{\lambda}_2 \\ & = o(\|\bar{\lambda}_1, \bar{\lambda}_2\|^2), \bar{\lambda}_1 - 62.45901316\bar{\lambda}_2 < 0\} \end{aligned}$$

6. Conclusion. The detailed bifurcation information on the improved endocrine model is presented under electromagnetic induction and external current in this paper. For external current and parameter k_0 , we use codimension-one and ISIs bifurcation to study the bifurcation structure. Numerical simulations show that the system realizes the transition between quiescence and firing state via Hopf bifurcation and fold bifurcation. As the I_{ext} increases, the system experiences three complex dynamical behaviors: period-adding bifurcation, inverse period-doubling bifurcation, and period-doubling bifurcation leading to chaos. It reveals that external forcing current may have significant influences on the improved endocrine model under the magnetic field, and the induced current plays the role of external forcing current. The numerical results show that the same discharge modes can be generated by induced current and external forced current when the coupling strength between magnetic flux and membrane potential is weak. Besides, we also analyze the different bursting patterns by fast-slow dynamics analysis. While the coupling strength between magnetic flux and membrane potential is strong, the neuron model exhibits the different types of electrical activities under different intensity of induced current. This indicates that the electrical activities of the model neuron are very sensitive to the response of induced current and stimulus current. Beyond that, we explore the region of oscillation activities by using two-parameter bifurcations and calculate the local topologically equivalent normal forms. If the fold bifurcation and Hopf bifurcation curve are too close, it is not easy to draw the homoclinic bifurcation curve. Nevertheless, we also discuss the dynamical properties near the Bogdanov-Takens bifurcation point in detail, and theoretically confirm the three bifurcation curves by using bifurcation theory and central manifold theorem. Our theoretical and numerical results may contribute to better understand the dynamical behavior and the mechanism of the endocrine neuron under the magnetic field and external current terms.

Acknowledgments. This work was supported by the National Natural Science Foundation of China under Grant Nos. 11872183 and 11572127.

REFERENCES

- [1] J. F. Barry, M. J. Turner, J. M. Schloss, D. R. Glenn, Y. Song, M. D. Lukin, H. Park and R. L. Walsworth, [Optical magnetic detection of single-neuron action potentials using quantum defects in diamond](#), *Proc. Natl. Acad. Sci. U.S.A.*, **113** (2016), 14133–14138.
- [2] R. Bertram and J. E. Rubin, [Multi-timescale systems and fast-slow analysis](#), *Math. Biol.*, **287** (2017), 105–121.
- [3] F. A. Carrillo, F. Verduzco and J. Delgado, [Analysis of the Takens-Bogdanov bifurcation on m-parameterized vector fields](#), *Internat. J. Bifur. Chaos Appl. Sci. Engrg.*, **20** (2010), 995–1005.
- [4] L. Duan, Q. Cao, Z. Wang and J. Su, [Dynamics of neurons in the pre-Bötzinger complex under magnetic flow effect](#), *Nonlinear Dynam.*, **94** (2018), 1961–1971.

- [5] L. Duan, Q. Lu and Q. Wang, [Two-parameter bifurcation analysis of firing activities in the Chay neuronal model](#), *Neurocomputing*, **72** (2008), 341–351.
- [6] H. Gu, [Experimental observation of transition from chaotic bursting to chaotic spiking in a neural pacemaker](#), *Chaos*, **23** (2013), 023126.
- [7] F. Han, Z. Wang, Y. Du, X. Sun and B. Zhang, [Robust synchronization of bursting Hodgkin-Huxley neuronal systems coupled by delayed chemical synapses](#), *Int. J. Non. Linear. Mech.*, **70** (2015), 105–111.
- [8] E. M. Izhikevich, [Neural excitability, spiking and bursting](#), *Internat. J. Bifur. Chaos Appl. Sci. Engrg.*, **10** (2000), 1171–1266.
- [9] M. S. Kafraj, F. Parastesh and S. Jafari, [Firing patterns of an improved Izhikevich neuron model under the effect of electromagnetic induction and noise](#), *Chaos, Solitons Fractals*, **137** (2020), 109782, 11 pp.
- [10] Y. A. Kuznetsov, *Elements of Applied Bifurcation Theory*, 3rd edition, Springer-Verlag, New York, 2004.
- [11] J. Li, Y. Wu, M. Du and W. Liu, [Dynamic behavior in firing rhythm transitions of neurons under electromagnetic radiation](#), *Acta Phys. Sin.*, **64** (2015), 030503.
- [12] Y. Loewenstein, S. Mahon, P. Chadderton, K. Kitamura, H. Sompolinsky, Y. Yarom and M. Häusser, [Bistability of cerebellar Purkinje cells modulated by sensory stimulation](#), *Nature Neurosci.*, **8** (2005), 202–211.
- [13] B. Lu, S. Liu, X. Liu, X. Jiang and X. Jang, [Bifurcation and spike adding transition in Chay-Keizer model](#), *Internat. J. Bifur. Chaos Appl. Sci. Engrg.*, **26** (2016), 1650090, 13 pp.
- [14] M. Lv and J. Ma, [Multiple modes of electrical activities in a new neuron model under electromagnetic radiation](#), *Neurocomputing*, **205** (2016), 375–381.
- [15] A. Mondal, R. K. Upadhyay, J. Ma et al., [Bifurcation analysis and diverse firing activities of a modified excitable neuron model](#), *Cognitive Neurodynamics*, **13** (2019), 393–407.
- [16] A. Mvogo, C. N. Takembo, H. P. Ekobena Fouda and T. C. Kofané, [Pattern formation in diffusive excitable systems under magnetic flow effects](#), *Phys. Lett. A*, **381** (2017), 2264–2271.
- [17] C. S. Nunemaker, R. Bertram, A. Sherman, K. Tsaneva-Atanasova, C. R. Daniel and L. S. Satin, [Glucose modulates \$\[Ca^{2+}\]_i\$ oscillations in pancreatic islets via ionic and glycolytic mechanisms](#), *Biophys. J.*, **91** (2006), 2082–2096.
- [18] J. Rinzel, [Bursting oscillations in an excitable membrane model](#), *Ordinary Partial Differ. Equations*, Springer Berlin Heidelberg, Berlin, Heidelberg **1151** (1985), 304–316.
- [19] J. E. Rubin, J. Signerska-Rynkowska, J. D. Touboul and A. Vidal, [Wild oscillations in a nonlinear neuron model with resets: \(I\) bursting, spike-adding and chaos](#), *Discrete. Contin. Dyn. Syst. Ser. B*, **22** (2017), 3967–4002.
- [20] A. Saito, T. Terai, K. Makino, M. Takahashi et al., [Real-time detection of stimulus response in cultured neurons by high-intensity intermediate-frequency magnetic field exposure](#), *Integr. Biol.*, **10** (2018), 442–449.
- [21] A. Saito, K. Wada, Y. Suzuki and S. Nakasono, [The response of the neuronal activity in the somatosensory cortex after high-intensity intermediate-frequency magnetic field exposure to the spinal cord in rats under anesthesia and waking states](#), *Brain Res.*, **1747** (2020), 147063.
- [22] W. Teka, K. Tsaneva-Atanasova, R. Bertram and J. Tabak, [From plateau to pseudo-plateau bursting: Making the transition](#), *Bull. Math. Biol.*, **73** (2011), 1292–1311.
- [23] K. Tsaneva-Atanasova, H. M. Osinga, T. Rieß and A. Sherman, [Full system bifurcation analysis of endocrine bursting models](#), *J. Theor. Biol.*, **264** (2010), 1133–1146.
- [24] X. J. Wang, [Genesis of bursting oscillations in the Hindmarsh-Rose model and homoclinicity to a chaotic saddle](#), *Phys. D*, **62** (1993), 263–274.
- [25] F. Zhan, S. Liu, X. Zhang, J. Wang and B. Lu, [Mixed-mode oscillations and bifurcation analysis in a pituitary model](#), *Nonlinear Dynam.*, **94** (2018), 807–826.

Received November 2020; 1st revision January 2021; 2nd revision March 2021.

E-mail address: wqx.edu@qq.com

E-mail address: mashqliu@scut.edu.cn

E-mail address: cheersnow@163.com